

PAPER • OPEN ACCESS

## A comparative study of NaI(Tl), CeBr<sub>3</sub>, and CZT for use in a real-time simultaneous nuclear and fluoroscopic dual-layer detector

To cite this article: Wilco J C Koppert *et al* 2019 *Phys. Med. Biol.* **64** 135012

View the [article online](#) for updates and enhancements.

**MR Safe**  
**4D Phantom**  
**for MRgRT**



**[modusQA]**

Accuracy. Confidence.™

[Learn More](#)

## OPEN ACCESS



## PAPER

# A comparative study of NaI(Tl), CeBr<sub>3</sub>, and CZT for use in a real-time simultaneous nuclear and fluoroscopic dual-layer detector

RECEIVED  
29 October 2018REVISED  
28 May 2019ACCEPTED FOR PUBLICATION  
3 June 2019PUBLISHED  
4 July 2019

Original content from this work may be used under the terms of the [Creative Commons Attribution 3.0 licence](#).

Any further distribution of this work must maintain attribution to the author(s) and the title of the work, journal citation and DOI.

Wilco J C Koppert<sup>1</sup>, Martijn M A Dietze<sup>1,2,3</sup> , Sandra van der Velden<sup>1,2</sup> , J H Leo Steenberg<sup>1</sup> and Hugo W A M de Jong<sup>1,2</sup><sup>1</sup> Radiology and Nuclear Medicine, Utrecht University and University Medical Center Utrecht, PO Box 85500, 3508 GA, Utrecht, The Netherlands<sup>2</sup> Image Sciences Institute, Utrecht University and University Medical Center Utrecht, PO Box 85500, 3508 GA, Utrecht, The Netherlands<sup>3</sup> Author to whom any correspondence should be addressed.E-mail: [m.m.a.dietze@umcutrecht.nl](mailto:m.m.a.dietze@umcutrecht.nl)Keywords: real-time hybrid imaging, gamma camera, SPECT, PMT, NaI(Tl), CeBr<sub>3</sub>, CZT

## Abstract

Simultaneous acquisition of nuclear and fluoroscopic projections could be of benefit for image-guided radionuclide administration. A gamma camera positioned behind an x-ray flat panel detector can accomplish such simultaneous acquisition, but the gamma camera performance suffers from the intense x-ray dose. A regular NaI(Tl)-based camera has nominal performance up to 0.02 nGy dose per pulse, whereas 10 nGy dose is expected for our foreseen applications. We evaluated the performance of CeBr<sub>3</sub>- and CZT-based detectors and investigated a cost-effective improvement of a regular NaI(Tl)-based camera by the introduction of a high-pass filter and shorting circuit.

A CeBr<sub>3</sub>-based detector was exposed to 5 mGy x-ray dose and the resulting light emission was measured over time to quantify the crystal afterglow, allowing comparison with a previously measured NaI(Tl)-based detector. The NaI(Tl)-, CeBr<sub>3</sub>- and CZT-based detectors were exposed to x-ray pulse sequences with dose from 0.06 to 60 nGy, while being irradiated with a gamma source. The mean gamma energy and energy resolution in between the x-ray pulses were measured as a reference of the detector performance.

The afterglow signal after 3 ms was 14.1% for the NaI(Tl)-based detector, whereas for the CeBr<sub>3</sub>-based detector it was only 0.1%. The limits for a proper functioning detectors are 0.32 nGy for the NaI(Tl)-based detector with high-pass filter and shorting circuit and 18.94 nGy for the one with CeBr<sub>3</sub>. No energy degradation was observed for the CZT module in the studied dose range.

The performance of regular NaI(Tl)-based gamma cameras deteriorates when exposed to high x-ray doses. CeBr<sub>3</sub> and CZT are much better suited for introduction into a dual-layer detector but have high associated costs. Addition of a high-pass filter and shorting circuit into the PMT of a NaI(Tl)-based detector is a cost-effective solution that works well for low dose levels.

## Introduction

Single-photon emission computed tomography (SPECT) has been combined with computed tomography (CT) in hybrid SPECT/CT scanners to provide attenuation correction and anatomical reference for nuclear images. The scans are conventionally acquired sequentially, i.e. a patient first undergoes SPECT imaging after which a CT scan is performed. We envision two situations in which simultaneous acquisition of nuclear and fluoroscopic images could be of benefit: (i) for guidance of radioisotope administration in an interventional setting (in e.g. radioembolization), inasmuch as direct feedback on the activity distribution with anatomical reference is obtained; and (ii) for improvement of SPECT image quality, by exploiting the anatomical information from the fluoroscopic images to correct for respiratory motion artifacts in the SPECT reconstruction.

There exist scanners on the market that could technically perform such simultaneous acquisition (e.g. the Brightview XCT developed by Philips Healthcare or systems in research (Kalki *et al* 1997)). However, these systems are too large to enable smooth integration in the intervention room (required for the guidance of radioisotope

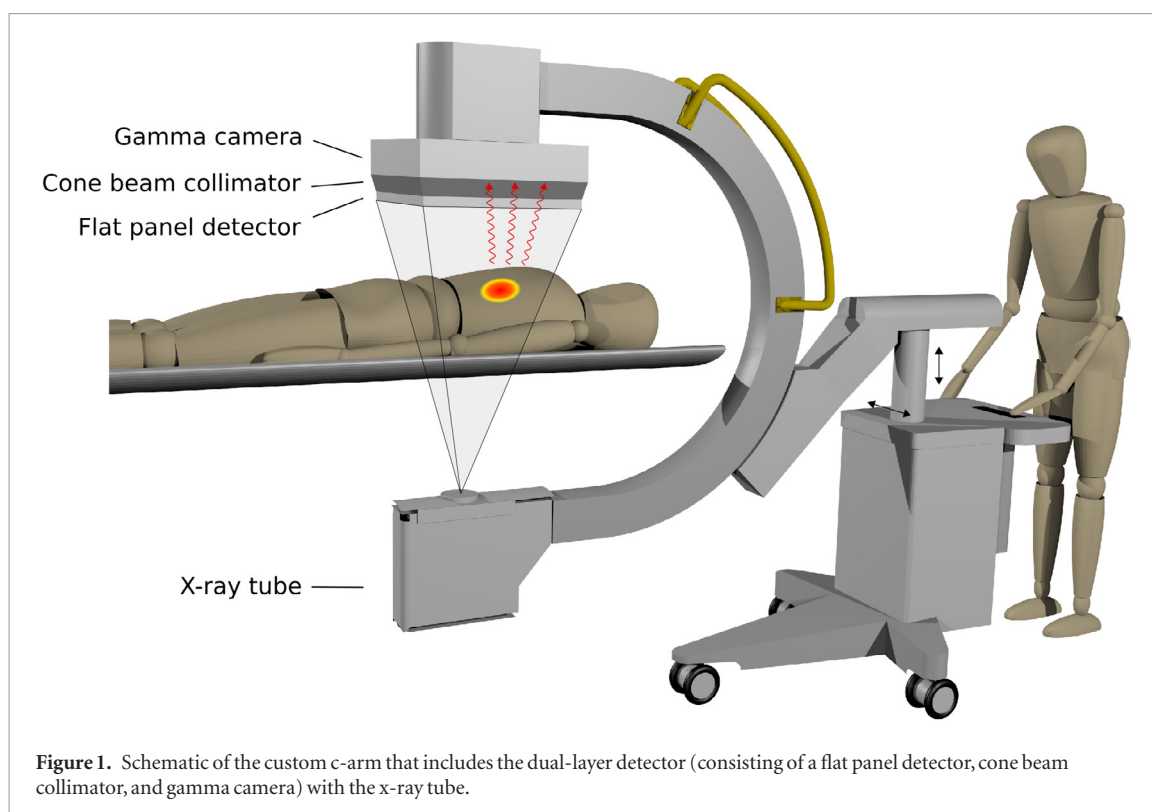


**Figure 1.** Schematic of the custom c-arm that includes the dual-layer detector (consisting of a flat panel detector, cone beam collimator, and gamma camera) with the x-ray tube.

administration) and the nuclear and fluoroscopic projections are captured under different angles, making simultaneous image interpretation difficult. In order to mitigate these problems, we have proposed a dual-layer detector (Dietze *et al*, Dietze *et al* 2019, Van der Velden *et al* 2019). The dual-layer detector consists of an x-ray flat panel detector, which is placed in front of a gamma camera mounted with cone beam collimator. By positioning the x-ray tube in the focal point of the cone beam collimator, fluoroscopic and nuclear projections capture the same field of view. This design has thus two advantages over the above mentioned systems: (i) the acquired fluoroscopic and nuclear projections intrinsically overlap, and (ii) the system can be manufactured considerably more compact and mobile by placing the detector on a custom c-arm (see figure 1 for an illustration).

The working principle of the dual-layer detector relies on the energy difference of the nuclear (gamma) and fluoroscopic (x-ray) photons. The most commonly used radioisotope in nuclear medicine ( $Tc^{99m}$ ) emits gamma photons at the relatively high energy of 140 keV. This allows a considerable fraction of photons to pass through the flat panel detector so that they are absorbed in the gamma camera. For the prototype system, in which the lead back shielding of the flat panel was thinned, the gamma photon transmission was approximately 55% (Van der Velden *et al* 2019). In contrast, the average energy of the photons from the x-ray tube with clinical fluoroscopy is typically in the order of 60 keV, making them predominantly captured in the flat panel detector.

Nevertheless, a non-negligible fraction of x-rays will penetrate the flat panel detector to be absorbed in the gamma camera. For the prototype system, this transmission factor was calculated to be approximately 2% at 80 kVp (Siemens). Although this fraction is thus not large, for clinical doses it gives rise to fluxes that are orders of magnitudes higher than what can be handled by a conventional gamma camera. In practice, such high detector doses result in an incorrect determination of photon energy and possibly incorrect photon location from the Anger logic (Koppert *et al* 2018).

These problems can partly be mitigated by performing interleaved measurements, exploiting the short duration of the x-ray pulses. At higher dose levels, however, the gamma camera performance also starts to deteriorate outside of the x-ray pulse time-window due to crystal afterglow. This means that more nuclear signal should be masked, up to the point that the effects become so severe that the gamma camera cannot be used at all. A regular NaI(Tl)-based camera was previously shown to be able to correctly handle dose levels of up to 0.02 nGy (Koppert *et al* 2018). For our application, however, doses in the range of 10 nGy per pulse are expected, and hence solutions for this problem should be found.

NaI(Tl) has been used as scintillating crystal in almost all traditional gamma cameras in the past decades but is known to suffer from severe afterglow. A more recently introduced crystal is  $CeBr_3$  (Guss *et al* 2009), of which one of the claimed key features is its fast response after gamma photon detection (<https://scionix.nl/scintillation-crystals>, Lecoq 2016). CZT semiconductor detectors are known for their high-rate detecting capabilities (Iwanczyk *et al* 2009, Hsieh *et al* 2018) and thus might also be beneficial for use in the dual-layer detector. The last two gamma detectors are unfortunately relatively expensive when used in a full-sized gamma camera. Therefore, a

**Table 1.** Properties of the gamma detectors as reported from literature ([www.crystals.saint-gobain.com/sites/imdf.crystals.com/files/documents/sodium-iodide-material-data-sheet\\_0.pdf](http://www.crystals.saint-gobain.com/sites/imdf.crystals.com/files/documents/sodium-iodide-material-data-sheet_0.pdf), [www.advatech-uk.co.uk/cebr3.html](http://www.advatech-uk.co.uk/cebr3.html)). Values denoted with \* are from our own measurements in absence of x-rays (for the PMTs: without high-pass filter). The energy resolution is defined as the FWHM of the fitted Gaussian function. The photopeak efficiency was determined from the number of counts inside the  $3\sigma$  photopeak window (see figure 7).

	NaI(Tl)	CeBr <sub>3</sub>	CZT
Detector	Scionix 51B51/2M	Scionix 51B10/2M	Kromek DMatrix
Energy resolution	7.6% (140 keV) *	8.1% (140 keV) *	3.6% (122 keV) *
Photopeak efficiency	79.9% (140 keV) *	88.1% (140 keV) *	50.4% (122 keV) *
Light yield	38 photons keV <sup>-1</sup>	60 photons keV <sup>-1</sup>	—
Decay time	250 ns	19 ns	—
Wavelength of max emission	415	380	—
Hygroscopic	Yes	Yes	No
Production	Easy	Difficult	Difficult
Cost	Low	High	High

more cost-effective solution, with the introduction of a high-pass filter and shorting circuit in the PMT circuitry in a regular NaI(Tl) gamma camera, is also explored.

The purpose of this study is to evaluate the performance of a NaI(Tl)-based detector with high-pass filter, a CeBr<sub>3</sub>-based detector, and a CZT module, when exposed to high x-ray fluxes, so that it can be determined which detectors are best suited for use in a simultaneous fluoroscopic and nuclear dual-layer detector.

## Methods

Three different gamma sensors were investigated for comparison: NaI(Tl)-, CeBr<sub>3</sub>-, and CZT-based. Their most important properties have been summarized in table 1. The dose on the detector was measured with the RaySafe (Unfors RaySafe, Billdal, Sweden) for all experiments. A schematic overview of the performed experiments can be found in figure 2.

### Afterglow quantification

Scintillation crystals may suffer from phosphorescence, due to the thermal release of trapped charges inside the crystal. This effect is often reported as afterglow in literature and deteriorates the gamma camera performance during and after intense x-ray exposure. We have previously quantified the magnitude of this afterglow for NaI(Tl) (Koppert *et al* 2018) by exposing the crystal to a single strong x-ray pulse of 20 mGy (120 kVp, 100 mA) for one second. The results from the mentioned study are reused in this manuscript, to allow for comparison with CeBr<sub>3</sub>.

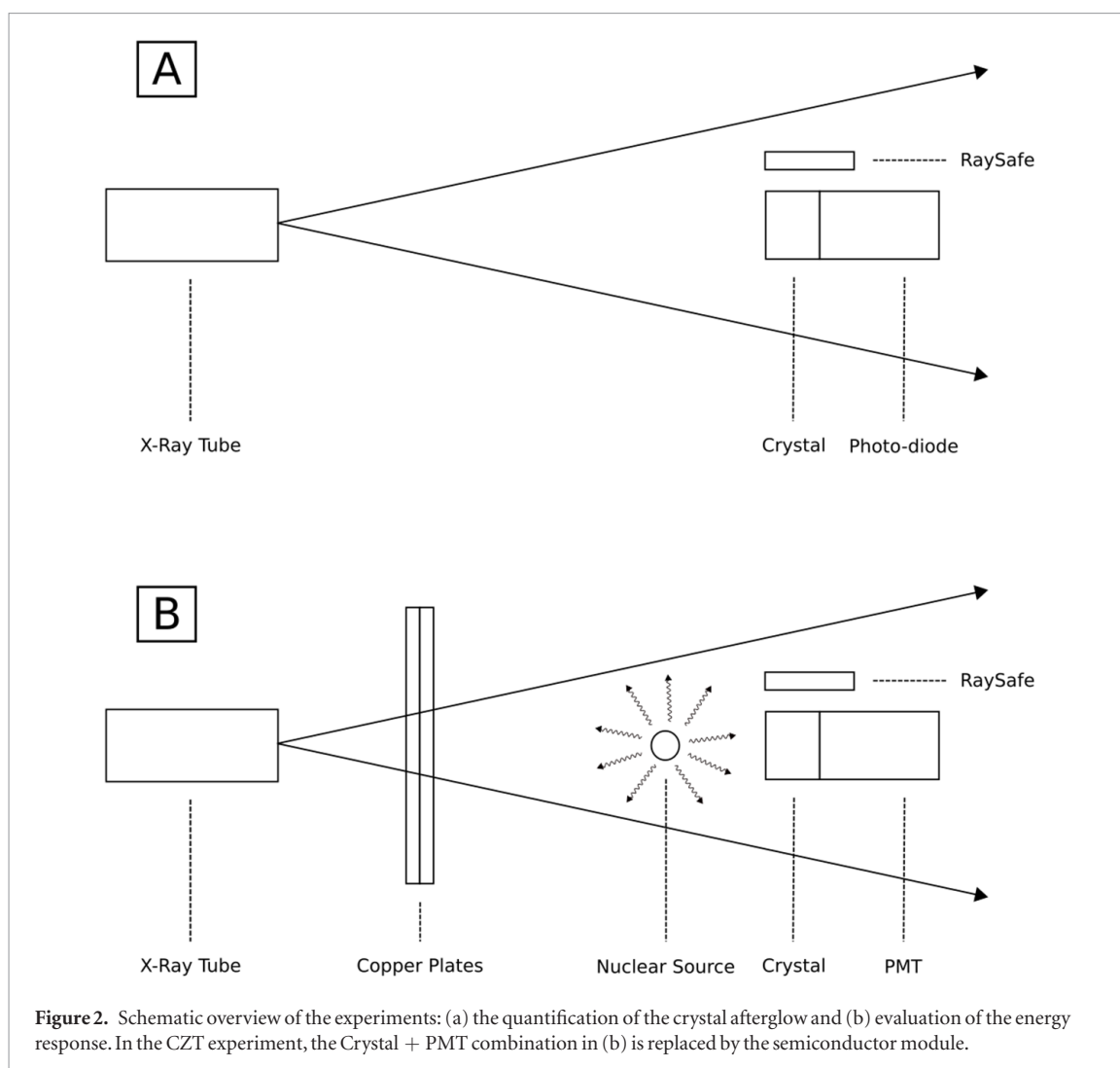
The afterglow intensity and decay time of CeBr<sub>3</sub> are reported to be small (<https://scionix.nl/scintillation-crystals>), however, no quantitative values were found in the literature. Hence, we performed the same afterglow measurement as with NaI(Tl) (Koppert *et al* 2018) by attaching a CeBr<sub>3</sub> crystal to a Hamamatsu S1227 silicon photo-diode and exposing it to a continuous x-ray pulse of 5 mGy (90 kVp, 80 mA) for one second. The detector configuration was the same as with the NaI(Tl) experiment, but a slightly lower dose was used for availability reasons.

### High-pass filter

In our previous work, it was found that the NaI(Tl) afterglow signal induced by high x-ray doses consisted of a reproducible stable background signal (Koppert *et al* 2018). This property was used to perform offline afterglow correction by subtracting the signal of a second measurement with an x-ray pulse but in absence of gamma photons. This two-step acquisition can be avoided by introducing a high-pass filter in the PMT signal processing circuitry, such that the gamma signals are automatically selected from the afterglow background signal.

Besides induction of crystal afterglow, high x-ray dose may also hamper proper PMT functioning when intense light induces large currents in the cathode. To minimize PMT saturation, an ETL 2" Type 9266 PMT was first modified by shorting the cathode with the first dynode for approximately 1 ms before the x-ray pulse to 1 ms after the pulse, temporarily reducing the PMT gain by approximately a factor of 30. The short was applied slightly longer than the duration of the x-ray pulse to ensure that small timing differences did not influence the results.

During the experiments, the PMT response was read out by an oscilloscope and the energies of the detected gamma photons were reconstructed by integration of the acquired signals when the short was not applied. Following the recommendations of our previous work (Koppert *et al* 2018), the high-pass filter was configured with 50 kHz cut-off frequency and the capacitances were reduced from 10 nF to 1 nF in the last three amplification stages.



The PMT with high-pass filter and shorting circuit was optically connected to a circular NaI(Tl) crystal (51 mm diameter and 51 mm thickness) or CeBr<sub>3</sub> crystal (51 mm diameter and 10 mm thickness). The cathode voltage was set to  $-400$  V and  $-512$  V for NaI(Tl) and CeBr<sub>3</sub>, respectively, to retrieve comparable pulse intensities for gamma photons.

### Detector comparison

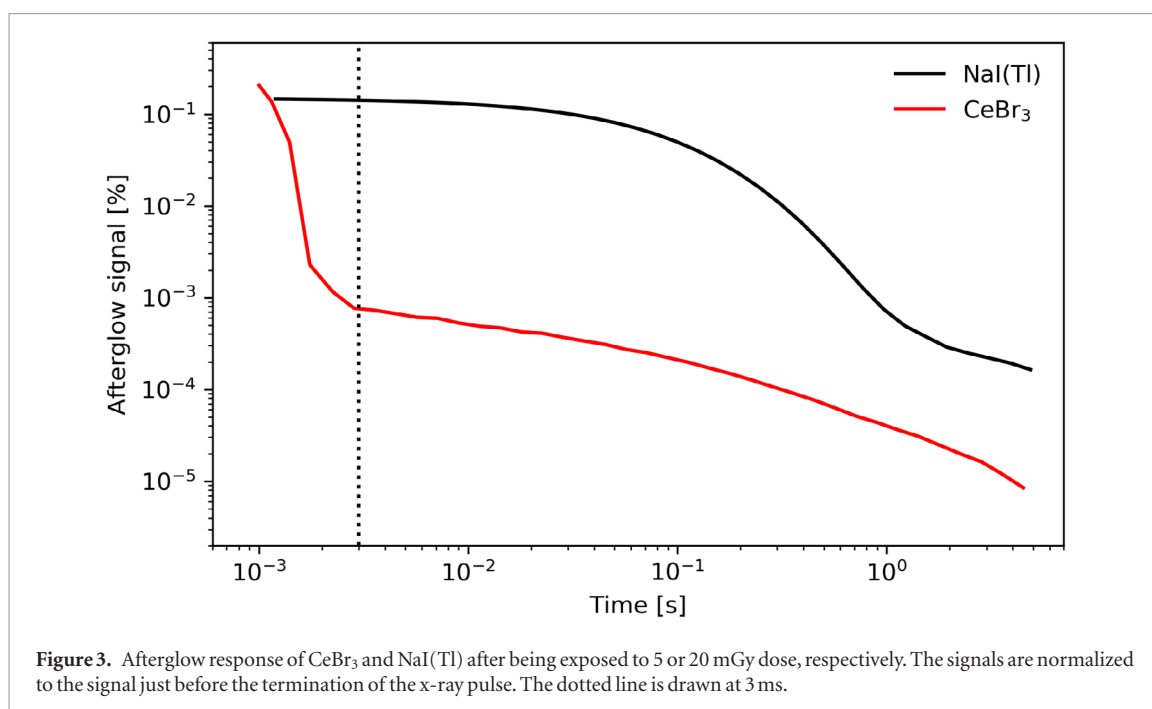
The NaI(Tl)- and CeBr<sub>3</sub>-based detectors were first exposed to a Tc<sup>99m</sup> source in absence of x-rays to retrieve the energy resolution without the influence of x-ray dose. Following this, the assemblies were exposed to approximately 5 s of x-ray pulses (80 kVp, 0.11 mA) of 10 ms duration at 15 Hz. Introducing copper plates with 8.0, 6.0, 4.9, or 4.0 mm between the detector and x-ray tube resulted in doses on the detector of 0.06, 0.32, 0.91, and 2.18 nGy for NaI(Tl). Because the CeBr<sub>3</sub>-based detector is expected to cope better with a high dose than NaI(Tl), it was also exposed to 4.29, 9.43, and 18.94 nGy (attenuation of 3.2, 2.6, and 2.0 mm copper, respectively). The energy resolution and mean energy of the Tc<sup>99m</sup> source were then again determined.

For CZT, a Co<sup>57</sup> point-source was positioned in front of a DMatrix detector module (Kromek, Sedgfield, United Kingdom) with 5 mm thickness and 2 mm pixel pitch, which was then exposed from 0.04 nGy (10 mm copper) to 60 nGy (2 mm copper) using the same x-ray pulses as above but now sampled at 3.75 Hz, due to availability reasons. The detector was shielded with lead, to avoid possible influence of x-rays on the read-out electronics.

## Results

### Afterglow quantification

The afterglow intensity, as a function of time, is shown in figure 3 for both NaI(Tl) and CeBr<sub>3</sub>. The signals are normalized to the signal height just before the termination of the x-ray pulse. Although the CeBr<sub>3</sub> experiment used 5 mGy instead of 20 mGy with the previous NaI experiment, the relative performance can be correctly



studied as the crystals had reached a saturation point. The afterglow signal after 3 ms was 14.1% for the NaI(Tl)-based detector, whereas for the CeBr<sub>3</sub>-based detector it was only 0.1%. We report the signal at 3 ms to allow for comparison with literature (e.g. (<https://scionix.nl/scintillation-crystals>, Lecoq 2016)).

### High-pass filter

The response over time, when exposed to a sequence of 2.18 nGy pulses, is shown in figure 4 for the NaI(Tl)-based detector with shorting circuit but without high-pass filter. Evident is that the signal had a major background component, which decayed exponentially towards the baseline. It took a few milliseconds before all dynode potentials were recovered when the shortage was turned off. The presence of Tc<sup>99m</sup> is visible in the small spikes on top of the background signal, which gives an indication of the relative size of the afterglow signal.

The response over time, when exposed to a sequence of 2.18 nGy pulses, is shown in figure 5 for the NaI(Tl)-based detector with shorting circuit and high-pass filter. If compared with figure 4, it is observed that the afterglow component is greatly reduced from the signal. The signal from the gamma photons now also contains a small positive overshoot, which is inherent to the use of the filter as the gamma signals contain also frequencies below the cut-off frequency.

### Detector comparison

The signal of the CeBr<sub>3</sub>-based detector, when exposed to a sequence of 2.18 nGy pulses, is shown in figure 6 for the PMT with shorting circuit but without high-pass filter. It is found to be substantially more stable, which is in agreement with the results from the afterglow measurement. A small background signal can however still be observed. The remainder of this work thus studied the performance CeBr<sub>3</sub> with the high-pass filter included.

Examples of the spectra of the studied detectors (without dose) are shown in figure 7. The energy resolution of the detectors in between x-ray pulses can be characterized by fitting a Gaussian to the collected gamma photon energies. The photopeak efficiency was calculated by dividing the number of counts inside the photopeak window at  $3\sigma$  with the total number of counts, which resulted in an efficiency of 79.9% for NaI(Tl), 88.1% for CeBr<sub>3</sub>, and 50.4% for CZT.

The obtained mean and corresponding energy resolution are collected in table 2 for the studied dose levels. For CZT only the measurements without dose and with 60.40 nGy have been reported, as slightly different doses were sampled than with the crystal-based detectors. No differing values were observed for the dose levels in between these two measurements.

The introduction of the high-pass filter resulted in an increase in energy resolution (full width at half maximum (FWHM) of the fitted Gaussian function) of approximately 2 percent point (pp), by comparing to the values obtained without high-pass filter in table 1. The dose levels where the deviation from the energy resolution without dose became larger than 1 percent point (pp) are 0.32 nGy for NaI(Tl) and 18.94 nGy for CeBr<sub>3</sub>. For CZT, no deviations were observed in the studied dose range. The threshold value of 1 pp was chosen because it was substantially larger than the variations observed between the measurements (e.g. approximately 0.2 pp for the first five measurements of CeBr<sub>3</sub>).

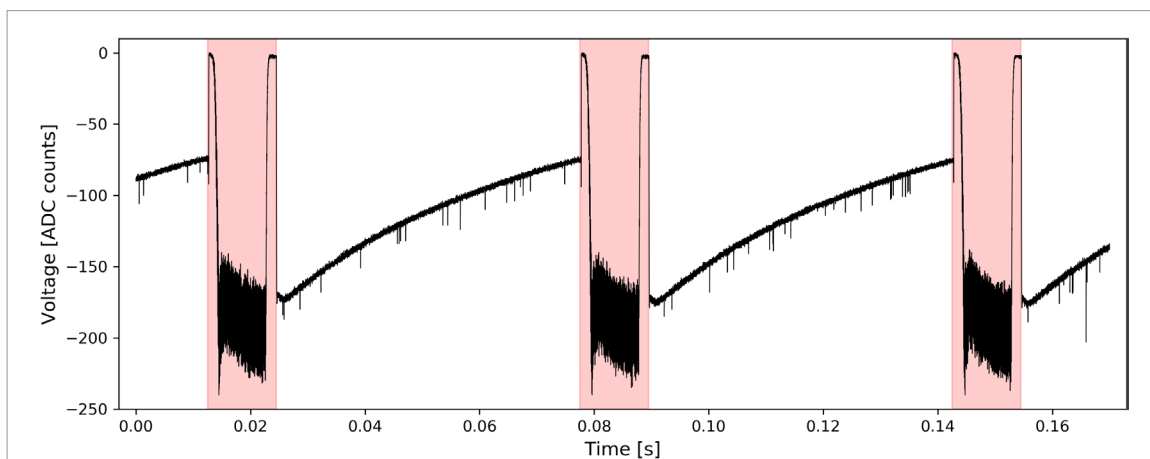


**Figure 4.** Raw signal over time of the NaI(Tl)-based detector with shorting circuit but without high-pass filter, when exposed to 2.18 nGy pulses. The red shaded regions denote the times when the short was applied.

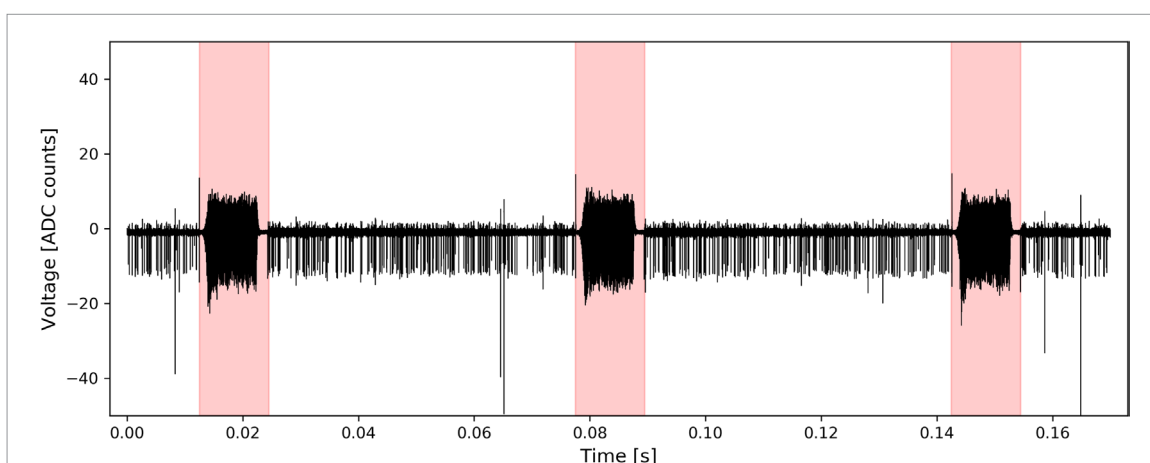


**Figure 5.** Raw signal over time of the NaI(Tl)-based detector with shorting circuit and high-pass filter, when exposed to 2.18 nGy pulses. The red shaded regions denote the times when the short was applied.

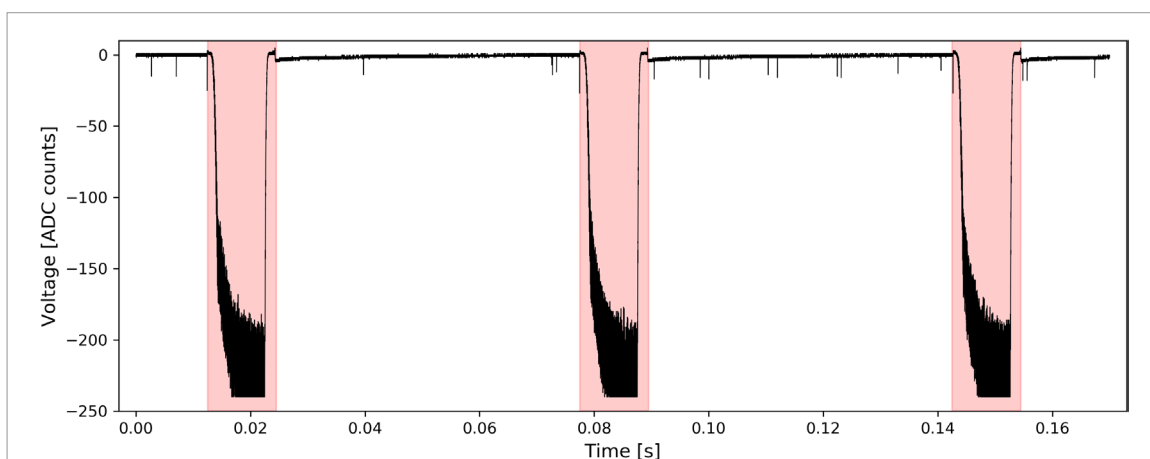


**Figure 6.** Raw signal over time of the CeBr<sub>3</sub>-based detector with shorting circuit but without high-pass filter, when exposed to 2.18 nGy pulses. The red shaded regions denote the times when the short was applied.

## Discussion

Regular NaI(Tl)-based gamma cameras cannot be used when exposed to high x-ray dose, which for instance occurs in a simultaneous nuclear and fluoroscopic imaging detector. This study reported on two detectors (CeBr<sub>3</sub> and CZT) that can better cope with the difficulty of high dose and a cost-effective solution for regular NaI(Tl)-based gamma cameras by the introduction of a high-pass filter and shorting circuit. The quantification of the afterglow magnitude for CeBr<sub>3</sub> has been reported for the first time.

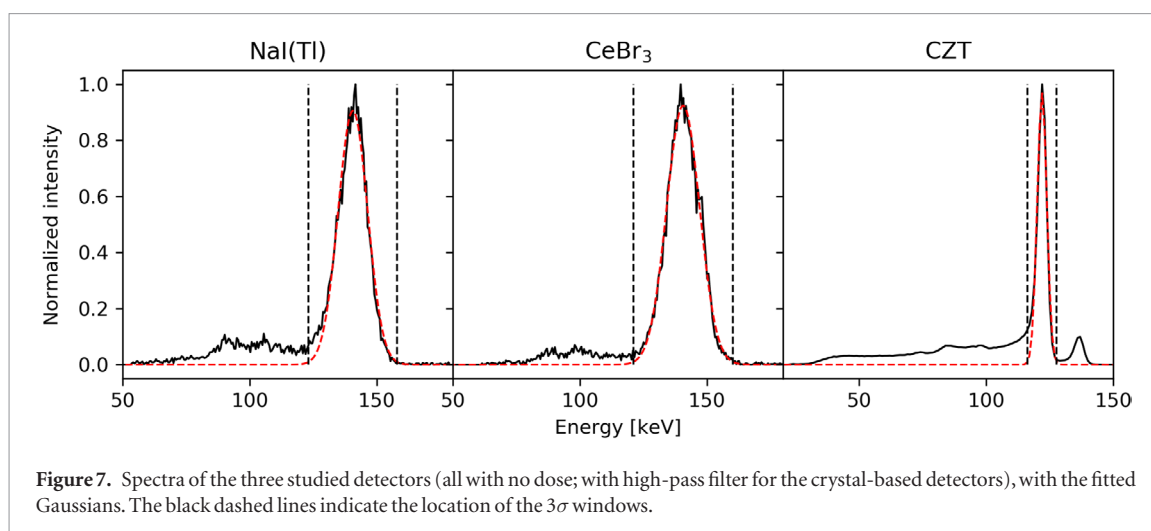


**Figure 7.** Spectra of the three studied detectors (all with no dose; with high-pass filter for the crystal-based detectors), with the fitted Gaussians. The black dashed lines indicate the location of the  $3\sigma$  windows.

**Table 2.** Mean energy in keV and corresponding energy resolution (FWHM of the fitted Gaussian function) for the three detectors, for the several dose levels. The gamma source of NaI(Tl) and CeBr<sub>3</sub> was Tc<sup>99m</sup> (140 keV), whereas the source was Co<sup>57</sup> (122 keV) for CZT. Marked in bold are the measurements where deviations larger than 1 percent point from the energy resolution without dose were observed.

Dose (nGy)	NaI(Tl)	CeBr <sub>3</sub>	CZT
No dose	140.6 ± 9.7%	140.7 ± 10.9%	121.4 ± 3.6%
0.06	139.5 ± 10.4%	141.4 ± 11.1%	.
0.32	<b>138.8 ± 11.4%</b>	141.1 ± 10.9%	.
0.91	<b>138.4 ± 13.5%</b>	140.9 ± 10.9%	.
2.18	<b>142.5 ± 17.3%</b>	140.4 ± 11.1%	.
4.92		140.8 ± 11.3%	.
9.43		140.6 ± 11.4%	.
18.94		<b>139.6 ± 12.2%</b>	.
60.40			121.4 ± 3.6%

The amount of dose on the gamma camera that would be present for the mentioned dual-layer detector largely depends on the used x-ray protocol and detector configuration. It is not finalized what settings will be used in clinical practice, but it is possible to make crude estimates on this matter. When an x-ray pulse (80 kVp, 0.52 mA) is attenuated by 20 cm of soft tissue, the prototype flat panel detector and the cone beam collimator, approximately 2.3 nGy is deposited on the gamma camera. Local depositions will, due to varying patient thickness, however, be higher. For now, we hence believe it will be necessary to make the gamma camera resistant to 10 nGy of x-ray dose.

It depends on the user and the performed procedure which magnitude of deterioration is acceptable. If a maximum deterioration of 1 pp in energy resolution is allowed to consider the gamma camera functioning correctly, the maximum dose levels on the detector were 0.32 nGy for the NaI(Tl)-based detector with high-pass filter and 18.94 nGy for one with CeBr<sub>3</sub>. No energy degradation was observed for the CZT module in the studied dose range. When considering the 10 nGy level as in the above paragraph, it is thus concluded that both CeBr<sub>3</sub> and CZT would be able to function our prototype dual-layer detector.

Other systems designed to simultaneously acquire simultaneous nuclear and fluoroscopic projections with the same field of view have also experienced difficulties with high incoming x-ray flux. For example, substantial influence of pile-up has been reported for the ETCT detector (Lang *et al* 1992), which could only be partially corrected for. The authors note the need for affordable, large scale CZT detectors. We reaffirm this statement with the results from our study.

There exist practical complications when introducing new detectors. Costs of CeBr<sub>3</sub> are expected to be more than a factor five higher than NaI(Tl). In addition, CeBr<sub>3</sub> crystals cannot be manufactured with large surfaces, which makes the production of a full-size gamma camera challenging. Although promising results have been claimed, the imaging capabilities of CeBr<sub>3</sub> are also largely undiscovered. CZT is increasingly available in large volumes and manufacturers are making significant progress in meeting the cost requirements for medical imaging. It is however not yet clear what will finally be achievable (Hugg *et al* 2017).

One other complication for CZT is the photopeak efficiency that was approximately 30 pp lower than that of NaI(Tl). This lower value is caused by charge sharing K-shell photons that escape the module, leading to a tail of lower energies in the energy spectrum (Trueb *et al* 2017). It might be that charge sharing effects can be mitigated

when introducing more complex data analysis algorithms (Wangerin *et al* 2011), but which efficiency can finally be achieved is not yet determined.

Although the introduction of the high-pass filter into the PMT was found to shift the maximum tolerated dose level, its introduction also caused an increase in energy resolution of approximately 2 pp compared to the configuration in absence of the filter. This effect was present in all measurements, thus also when the module was not exposed to x-rays. It is believed that this deterioration comes from the filtering of gamma related frequency components, making the signal response slightly more prone to fluctuations. More variability is, however, preferred over a systematically changing mean energy (as would be the case for the PMTs without the high-pass filter).

The shorting window for the measurements of gamma photons was set to 1 ms before and after the x-ray pulse to ensure that potential small timing differences did not influence the measurements. This extra 1 ms window caused a signal loss of approximately 3.5% ( $2 \times 1 \text{ ms} \times 15 \text{ Hz} = 30 \text{ ms}$  out of 850 ms measurement time). No systematic study on the optimal value to use for this window was performed. It might be that a shorter window (with lower signal loss) could also provide accurate results. However, since the signal loss at 1 ms was already relatively low, we did not perform further optimization in this work.

There may exist a relation between the energy resolution and the point of measurement in time because the afterglow component is predominately present just after the termination of a x-ray pulse. It thus might be possible to improve the energy resolution by rejecting a fraction of the gamma photons following the x-ray pulse. We, however, expect that for accurate imaging the number of nuclear counts is of greater importance than a slight improvement in energy resolution. Hence, we have not further studied this form of data processing in this work.

The afterglow has been reported at 3 ms because this is often done in literature and hence allows for comparison with other studies. For x-ray imaging, an afterglow level of less than 0.1% is generally required at 3 ms to ensure that no artifacts occur (Lecoq 2016). The requirements for simultaneous nuclear and fluoroscopic imaging are not yet clear because these are heavily dependent on the choice of x-ray protocol. The afterglow signal at 3 ms should ideally be low if a fast pulsed acquisition is used (e.g. 15 Hz), since too much signal would be corrupted otherwise. More deterioration may, however, be allowed if fewer x-ray pulses are used.

The afterglow signal measured in the photo-diode configuration cannot directly be related to that from a PMT, for instance because the detectors possess a different spectral sensitivity. The photo-diode measurement was included because the photo-diode is able to handle much higher dose levels compared to the PMT (which quickly saturates). Hence, this allowed to study the afterglow signal separately from any PMT deteriorating effects. Although not quantified, figures 4 and 6 give an indication of the magnitude of afterglow in the PMT configuration.

There exists a trade-off in which cut-off frequency to use for the high-pass filter. A high cut-off frequency reduces signal amplitude and thus reduces the energy resolution. A low cut-off frequency increases the decay time of the overshoot and increases the pile-up rate. For the measurements, it was decided to use 50 kHz, because this is well below the dominant frequencies as contained by the gamma signals and well above the background signal expected from afterglow effects.

It was found that the response of the mean energy and energy resolution do not behave systematically when exposed to increasing x-ray dose. For instance, the photopeak energy decreases and then jumps up again for the NaI(Tl)-based detector with high-pass filter. This effect is likely due to internal PMT saturation effects that are hard to predict and behave non-linearly.

## Conclusion

For our simultaneous nuclear and fluoroscopic prototype detector, x-ray dose on the gamma camera is expected to be in the order of 10 nGy. Regular NaI(Tl)-based gamma cameras have an accurate response up to 0.02 nGy and thus cannot be used in clinical practice. Detectors based on CeBr<sub>3</sub> and CZT have a good performance of up to 18.94 nGy and over 60 nGy, respectively, but have a much higher cost for large field of view cameras. Addition of a high-pass filter and shorting circuit in the PMT circuitry of regular NaI(Tl) cameras shifts the level of accurate performance up to 0.32 nGy, which may be a cost-effective solution for low x-ray doses.

## Acknowledgments

We thank PEO Radiation Technology (Wijchen, The Netherlands), Kromek (Sedgefield, United Kingdom), Philips Healthcare (Best, The Netherlands), and Scionix (Bunnik, The Netherlands) for the enlightening discussions and comprehensive support.

## Disclosure

This work is part of the STW-VIDI research program with project number 12977, which is (partly) financed by the Netherlands Organization for Scientific Research (NWO).

This project has received funding from the European Research Council (ERC) under the European Union's Horizon 2020 research and innovation program grant agreement No 646734.

## ORCID iDs

Martijn M A Dietze  <https://orcid.org/0000-0003-1159-3510>

Sandra van der Velden  <https://orcid.org/0000-0002-8054-0175>

## References

- Dietze M M A, Bastiaannet R, Kunnen B, Van der Velden S, Lam M G E H, Viergever M A and De Jong H W A M Respiratory motion compensation in interventional liver SPECT using simultaneous fluoroscopic and nuclear imaging *Med. Phys.* (accepted) (<https://doi.org/10.1002/mp.13653>)
- Dietze M M A, Kunnen B, Van der Velden S, Steenbergen J H L, Koppert W J C, Viergever M A and De Jong H W A M 2019 Performance of a dual-layer scanner for hybrid SPECT/CBCT *Phys. Med. Biol.* **64** 105020
- Guss P, Reed M, Yuan D, Reed A and Mukhopadhyay S 2009 CeBr<sub>3</sub> as a room-temperature, high-resolution gamma-ray detector *Nucl. Instrum. Methods Phys. Res. A* **608** 297–304
- Hsieh S S, Rajbhandary P L and Pelc N J 2018 Spectral resolution and high-flux capability tradeoffs in CdTe detectors for clinical CT *Med. Phys.* **45** 1433–43  
<https://scionix.nl/scintillation-crystals> (Accessed: 1 March 2019)
- Hugg J W, Harris B W and Radley I 2017 Affordable CZT SPECT with dose-time minimization *Proc. SPIE* **10132** 101321K
- Iwanczyk J S, Nygård E, Meirav O, Arenson J, Barber W C, Hartsough N E, Malakhov N and Wessel J C 2009 Photon counting energy dispersive detector arrays for x-ray imaging *IEEE Trans. Nucl. Sci.* **56** 535–42
- Kalki K, Blankespoor S C, Brown J K, Hasegawa B H, Dae M W, Chin M and Stillson C 1997 Myocardial perfusion imaging with a combined x-ray CT and SPECT system *J. Nucl. Med.* **38** 1535–40
- Koppert W J C, Van der Velden S, Steenbergen J H L and De Jong H W A M 2018 Impact of intense x-ray pulses on a NaI(Tl)-based gamma camera *Phys. Med. Biol.* **63** 065006
- Lang T F *et al* 1992 Description of a prototype emission transmission computed tomography imaging system *J. Nucl. Med.* **33** 1881–7
- Lecoq P 2016 Development of new scintillators for medical applications *Nucl. Instrum. Methods Phys. Res. A* **809** 130–9
- Siemens Simulation of x-ray spectra [www.oem-xray-components.siemens.com/x-ray-spectra-simulation](http://www.oem-xray-components.siemens.com/x-ray-spectra-simulation) (Accessed: 1 March 2019)
- Trueb P, Zamboni P and Broennimann C 2017 Assessment of the spectral performance of hybrid photon counting x-ray detectors *Med. Phys.* **44** 207–14
- Van der Velden S *et al* 2019 A dual-layer detector for simultaneous fluoroscopic and nuclear imaging *Radiology* **290** 833–8
- Wangerin K, Du Y and Jansen F 2011 CZT performance for different anode pixel geometries and data corrections *Nucl. Instrum. Methods Phys. Res. A* **648** S37–S41  
[www.advatech-uk.co.uk/cebr3.html](http://www.advatech-uk.co.uk/cebr3.html) (Accessed: 1 March 2019)  
[www.crystals.saint-gobain.com/sites/imdf.crystals.com/files/documents/sodium-iodide-material-data-sheet\\_0.pdf](http://www.crystals.saint-gobain.com/sites/imdf.crystals.com/files/documents/sodium-iodide-material-data-sheet_0.pdf) (Accessed: 1 March 2019)